



HAL
open science

The first comprehensive dataset of beyond-Voigt line-shape parameters from ab initio quantum scattering calculations for the HITRAN database: He-perturbed H₂ case study

P. Wcislo, Franck Thibault, N. Stolarczyk, H. Józwiak, M. Słowiński, M. Gancewski, K. Stankiewicz, M. Konefal, S. Kassi, A. Campargue, et al.

► To cite this version:

P. Wcislo, Franck Thibault, N. Stolarczyk, H. Józwiak, M. Słowiński, et al.. The first comprehensive dataset of beyond-Voigt line-shape parameters from ab initio quantum scattering calculations for the HITRAN database: He-perturbed H₂ case study. *Journal of Quantitative Spectroscopy and Radiative Transfer*, 2021, 260, pp.107477. 10.1016/j.jqsrt.2020.107477 . hal-03130375

HAL Id: hal-03130375

<https://hal.science/hal-03130375>

Submitted on 18 Feb 2021

HAL is a multi-disciplinary open access archive for the deposit and dissemination of scientific research documents, whether they are published or not. The documents may come from teaching and research institutions in France or abroad, or from public or private research centers.

L'archive ouverte pluridisciplinaire **HAL**, est destinée au dépôt et à la diffusion de documents scientifiques de niveau recherche, publiés ou non, émanant des établissements d'enseignement et de recherche français ou étrangers, des laboratoires publics ou privés.

HIGHLIGHTS

- new method for populating line-by-line spectroscopic databases with beyond-Voigt lineshape parameters
- He-perturbed H₂
- ab initio quantum scattering calculations of beyond-Voigt line-shape parameters
- simple and compact formula that allows the speed-dependence parameters to be calculated directly from the generalized spectroscopic cross sections
- dataset compatible with the HITRAN database
- temperature dependences of the beyond-Voigt line-shape parameters covering the range from 20 to 1000 K

Journal Pre-proof

The first comprehensive dataset of beyond-Voigt line-shape parameters from *ab initio* quantum scattering calculations for the HITRAN database: He-perturbed H₂ case study

P. Weislo,^{1,*} F. Thibault,² N. Stolarczyk,¹ H. Jóźwiak,¹ M. Słowiński,¹ M. Gancewski,¹
K. Stankiewicz,¹ M. Konefał,^{1,3} S. Kassı,³ A. Campargue,³ Y. Tan,⁴ J. Wang,⁴
K. Patkowski,⁵ R. Ciuryło,¹ D. Lisak,¹ R. Kochanov,⁶ L.S. Rothman,⁶ and I.E. Gordon⁶

¹*Institute of Physics, Faculty of Physics, Astronomy and Informatics,
Nicolaus Copernicus University in Torun, Grudziadzka 5, 87-100 Torun, Poland*

²*Univ Rennes, CNRS, IPR (Institut de Physique de Rennes)-UMR 6251, F-35000 Rennes, France*

³*University of Grenoble Alpes, CNRS, LIPhy, F-38000 Grenoble, France*

⁴*Hefei National Laboratory for Physical Sciences at Microscale, iChEM,
University of Science and Technology of China, Hefei, 230026 China*

⁵*Department of Chemistry and Biochemistry, Auburn University, Auburn, AL 36849, USA*

⁶*Harvard-Smithsonian Center for Astrophysics, Atomic and Molecular Physics Division, Cambridge, MA, USA*

(Dated: December 11, 2020)

We demonstrate a new method for populating line-by-line spectroscopic databases with beyond-Voigt line-shape parameters, which is based on *ab initio* quantum scattering calculations. We report a comprehensive dataset for the benchmark system of He-perturbed H₂ (we cover all the rovibrational bands that are present in the HITRAN spectroscopic database). We generate the entire dataset of the line-shape parameters (broadening and shift, their speed dependence, and the complex Dicke parameter) from fully *ab initio* quantum-scattering calculations. We extend the previous calculations by taking into account the centrifugal distortion for all the bands and by including the hot bands. The results are projected on a simple structure of the quadratic speed-dependent hard-collision profile. We report a simple and compact formula that allows the speed-dependence parameters to be calculated directly from the generalized spectroscopic cross sections. For each line and each line-shape parameter, we provide a full temperature dependence within the double-power-law (DPL) representation, which makes the dataset compatible with the HITRAN database. The temperature dependences cover the range from 20 to 1000 K, which includes the low temperatures relevant for the studies of the atmospheres of giant planets. The final outcome from our dataset is validated on highly accurate experimental spectra collected with cavity ring-down spectrometers. The methodology can be applied to many other molecular species important for atmospheric and planetary studies.

I. INTRODUCTION

The collisional line-shape effects, including the beyond-Voigt effects [1–8], play an important role in atomic and molecular physics [9–13]. On one hand, they give access to studying the molecular interactions [14–16] and dynamics [17], but on the other hand they can affect the accuracy of optical metrology based on molecular spectroscopy [18]. In particular, insufficient modeling of the line-shape effects can limit the accuracy of simulations of atmospheric measurements of the Earth [19] and other planets [20] and even modify the retrieved opacity of exoplanetary atmospheres [21, 22]. To address this problem, a new relational structure [23] was introduced into the most widely used line-by-line spectroscopic database, HITRAN [24], allowing the beyond-Voigt line-shape effects to be represented [25]. It is, however, remarkably challenging to populate the entire database (all the molecules and their isotopologues over a great spectral range and thermodynamic conditions) with purely experimental beyond-Voigt line-shape parameters, not only

due to a large number of transitions to be measured at different conditions and different spectral ranges, but also due to strong numerical correlations between the line-shape parameters.

In this article, we demonstrate a new method for populating line-by-line spectroscopic databases with beyond-Voigt line-shape parameters that is based on *ab initio* quantum scattering calculations. We report a comprehensive dataset for the benchmark system of He-perturbed H₂ lines. We cover all the rovibrational bands (with their branches) that are present in HITRAN. We generate the values of the line-shape parameters (broadening and shift, their speed dependence, and the complex Dicke parameter) from fully *ab initio* quantum-scattering calculations. We extend the calculations of the generalized spectroscopic cross sections reported in Refs. [15, 26] by taking into account the centrifugal distortion for all the bands and by including the hot bands. We extrapolate the *ab initio* results to populate very weak lines, i.e., higher overtones, $v' \geq 6$, higher rotational numbers, $J' \geq 8$, and high- v' hot bands, $v' \geq 6$; following the standard HITRAN notation, we denote the final and initial states of a transition with primes and double primes, respectively. The results are projected on a simple structure of the quadratic speed-dependent

* piotr.weislo@umk.pl

hard-collision (qSDHC) profile [27–29] that is consistent with the recently recommended HITRAN parametrization [30]. We also report a simple and compact formula that allows the speed-dependence parameters (within the quadratic model) to be calculated directly from the generalized spectroscopic cross sections, which considerably speeds up the calculations and makes them numerically more stable. For each line and each line-shape parameter we provide a full temperature dependence within the double-power-law (DPL) representation, which was recently recommended for the HITRAN database [30]. The results are valid for a wide temperature range from 20 to 1000 K, with the 50 - 200 K range prioritized (in this range the DPL fits have 10 times larger weights), which is relevant for the studies of the atmospheres of giant planets. The final outcome from our dataset is validated on highly accurate experimental spectra collected with cavity ring-down spectrometers [31] demonstrating sub-percent agreement. Incorporation of beyond-Voigt line-shape parameters reported in this paper together with their DPL temperature dependences into the HITRAN database is possible thanks to the recently developed flexible relational structure of HITRAN [23]. The complex structure of this dataset is easily accessible for non-expert HITRAN users thanks to the HITRAN Application Programming Interface (HAPI) [32] that automatically generates spectra at the desired spectral range and thermodynamic conditions chosen by the user.

The atmospheres of the giant planets in the Solar System are greatly dominated by a mixture of molecular hydrogen and atomic helium. Moreover, atmospheres of some types of super-Earth exoplanets are predicted to be dominated by the H₂-He mixture [21]. The spectroscopic studies of giant planet atmospheres are naturally based on the main isotopologue of molecular hydrogen [33]. However, although the abundance of hydrogen deuteride is 4 - 5 orders of magnitude smaller, HD is noticeable in the spectroscopic studies of giant planets [20, 33] due to the much larger intensity of the dipole transitions compared to the weak quadrupole lines in H₂. In total, four combinations of collision partners should be considered to provide a complete reference data for the planetary studies: self-perturbed H₂, He-perturbed H₂, H₂-perturbed HD and He-perturbed HD. In this article, we consider the simplest benchmark case of He-perturbed H₂.

In Section II, we discuss the general methodology of generating beyond-Voigt line-shape parameters from *ab initio* calculations. Section III illustrates the methodology on the examples of two rovibrational lines in He-perturbed H₂. The full comprehensive dataset for He-perturbed H₂ is discussed in Sec. IV and the complete dataset is provided in the supplementary material [34].

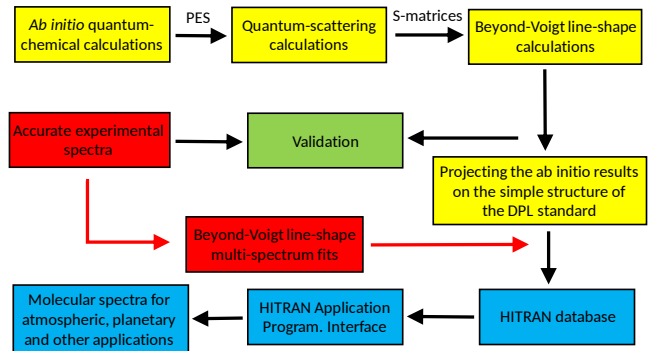


FIG. 1. Diagram illustrating our approach to generating the experimentally validated *ab initio* dataset of the beyond-Voigt line-shape parameters and its incorporation into the HITRAN database. The red arrows show the usual way of populating the database based on experimental spectra analysis only.

II. METHODOLOGY OF GENERATING DATASETS OF THE BEYOND-VOIGT LINE-SHAPE PARAMETERS BASED ON THE AB INITIO CALCULATIONS

A typical approach to populating the HITRAN database with the beyond-Voigt line-shape parameters [24, 32] uses the data that were obtained from fitting the advanced profiles to the high-quality experimental spectra [25, 35–39], see the red boxes in the flowchart in Fig. 1. It is a challenging task to populate the entire database with the purely experimental approach due to the large number of transitions required to be accurately measured at different conditions. Another difficulty is related to strong numerical correlations between the line-shape parameters, which often results in large systematic errors in the retrieved line-shape parameters. The numerical correlation can be considerably reduced by implementing the multispectrum fitting approach [40–42] which is, however, very demanding from a technical point of view and is still difficult to automatically apply to large experimental datasets.

In this article, we present a new methodology for populating the spectroscopic databases based on *ab initio* calculations. A key factor that enables development of this approach was a demonstration that the fully *ab initio* quantum-scattering calculations can reproduce the shapes of the high-quality collision-perturbed experimental spectra at the subpercent level [31], including the deep non-Voigt regime (by subpercent agreement we mean that the root-mean-square error of the *ab initio* model relative to profile peak (rRMSE) calculated within \pm FWHM is smaller than 1%). The flowchart in Fig. 1 illustrates our methodology (see the yellow boxes). The chain of the *ab initio* calculations starts with the quantum-chemical calculations of the PESs [14, 15]. In the second step, the PESs are used to perform the quantum-scattering calculations by solving the

close-coupling equations, which provide the scattering S-matrices as a function of relative kinetic energy of the collision, E_{kin} . The S-matrices allow us to calculate the generalized spectroscopic cross-sections, $\sigma_\lambda^q(E_{kin})$, that describe the collision perturbation of the optical coherence associated with the considered molecular transition. This approach also allows for the calculations of off-diagonal generalized spectroscopic cross-sections. Thus, for instance, the well-known case of overlapping lines could be considered. However, in this study we limit the discussion to the case of isolated lines, which is relevant for the molecular system considered here at pressures typical for the atmospheres of gas giants. We consider two types of generalized cross-sections that differ by the rank of the velocity tensor, λ . For the zero rank, $\lambda = 0$, σ_λ^q describes perturbation of internal motion of the molecule, and its real and imaginary parts have spectroscopic interpretation of the pressure broadening and shift cross-sections (PBXS and PSXS, respectively) [43–46]. For $\lambda = 1$, σ_λ^q describes perturbation of translational motion (including the correlations with dephasing and state-changing collisions) and it has spectroscopic interpretation of the complex Dicke cross-section (its real and imaginary parts are denoted as RDXS and IDXS, respectively) [26, 47–50]. q is the tensor rank of the spectral transition operator (equal to 1 and 2 for dipole and quadrupole lines, respectively). In principle, σ_λ^q should also be labeled with the quantum numbers specifying the ground and excited levels of the transition (a diagonal cross-section in Liouville space); for the sake of notation clarity we skip them in this article. The two complex cross sections, σ_0^q and σ_1^q , allow us to calculate the collisional quantities that are needed for modeling the beyond-Voigt shapes of molecular lines, as depicted in the third yellow box in Fig. 1. The basic quantities are the collisional broadening, γ , and shift, δ , of molecular lines expressed as a function of active molecule speed, v , which can be calculated as [3, 51]

$$\gamma(v) + i\delta(v) = \frac{1}{2\pi c} \frac{1}{k_B T} \frac{2}{\sqrt{\pi} v \bar{v}_p} \int_0^\infty dv_r v_r^2 e^{-\frac{v^2 + v_r^2}{\bar{v}_p^2}} \sinh\left(\frac{2vv_r}{\bar{v}_p^2}\right) \sigma_0^q(v_r), \quad (1)$$

where \bar{v}_p and v_r are the most probable speed of the perturber distribution and relative absorber-perturber speed, respectively. k_B and T are the Boltzmann constant and temperature. Two other line-shape parameters, which quantify the rate of the velocity-changing collisions, are the real, $\tilde{\nu}_{opt}^r$, and imaginary, $\tilde{\nu}_{opt}^i$, parts of the complex Dicke parameter, $\tilde{\nu}_{opt}$, which is calculated

as

$$\tilde{\nu}_{opt} = \tilde{\nu}_{opt}^r + i\tilde{\nu}_{opt}^i = \frac{1}{2\pi c} \frac{1}{k_B T} \langle v_r \rangle M_2 \times \int_0^\infty dx x e^{-x} \left[\frac{2}{3} x \sigma_1^q(E_{kin} = x k_B T) - \sigma_0^q(E_{kin} = x k_B T) \right], \quad (2)$$

where $M_2 = m_2/(m_1 + m_2)$, and m_1 and m_2 are the masses of the active and perturbing molecules (or atoms), $\langle v_r \rangle = \sqrt{8k_B T/\pi\mu}$ is the average relative speed and μ is the reduced mass of the colliding partners. The variable of integration, x , is a dimensionless kinetic energy of a collision, $x = E_{kin}/(k_B T)$. The quantities expressed by Eqs. (1) and (2) [i.e., $\gamma(v)$, $\delta(v)$, $\tilde{\nu}_{opt}^r$ and $\tilde{\nu}_{opt}^i$] carry all the collisional information that comes from our *ab initio* calculations and enters the beyond-Voigt line-shape models. The details of the line-shape calculations based on these quantities can be found in Ref. [6, 52, 53].

From the perspective of spectroscopy applications and populating the HITRAN database, the full speed dependences, given by Eq. (1), and full *ab initio* line-shape models [53] are far too complex to be stored in the database and are computationally too demanding to be used to analyze large sets of molecular spectra. Therefore, following Ref. [30], we project the full *ab initio* line-shape model on a simple structure of the quadratic speed-dependent hard-collision model (qSDHC) [27–29], in which the speed dependence is approximated with a quadratic function [54]

$$\gamma(v) + i\delta(v) \approx \gamma_0 + i\delta_0 + (\gamma_2 + i\delta_2) (v^2/v_m^2 - 3/2), \quad (3)$$

where v_m is the most probable absorber speed. The speed-averaged broadening and shift, γ_0 and δ_0 , are calculated as real and imaginary parts of a simple average of σ_0^q over the Maxwellian E_{kin} distribution [3, 51]

$$\gamma_0 + i\delta_0 = \frac{1}{2\pi c} \frac{1}{k_B T} \langle v_r \rangle \int_0^\infty dx x e^{-x} \sigma_0^q(E_{kin} = x k_B T). \quad (4)$$

Alternatively, γ_0 and δ_0 can be calculated by averaging $\gamma(v)$ and $\delta(v)$ over the Maxwell distribution of active molecule speed, v , yielding exactly the same result as Eq. (4). The two parameters quantifying the speed dependence of the broadening and shift, γ_2 and δ_2 , are calculated by demanding that the slope of the quadratic approximation equals the slope of the actual speed dependences at $v = v_m$ [53],

$$\gamma_2 + i\delta_2 = \frac{v_m}{2} \frac{d}{dv} (\gamma(v) + i\delta(v)) \Big|_{v=v_m}. \quad (5)$$

Following the generalized Hess method [4, 48, 50], we directly take the complex Dicke parameter, $\tilde{\nu}_{opt} = \tilde{\nu}_{opt}^r + i\tilde{\nu}_{opt}^i$, as a complex rate of the velocity-changing collisions in the qSDHC model [30]. In the cases of molecules

for which the Dicke narrowing is pronounced, we recommend the use of the β correction [25, 55] that improves the hard-collision approximation without increasing the cost of the line-shape computations. Note that the β correction is a generic concept valid for any molecular system and does not require any additional parameter to be stored (it depends only on the perturber-to-absorber mass ratio [55]). In total, the most general form of the qSDHC profile requires six line-shape parameters to be stored:

$$\gamma_0, \delta_0, \gamma_2, \delta_2, \tilde{\nu}_{\text{opt}}^r, \tilde{\nu}_{\text{opt}}^i. \quad (6)$$

The recent approach adopted in HITRAN [30] allows the temperature dependences of all the six line-shape parameter to be represented with the double-power-law (DPL):

$$\begin{aligned} \gamma_0(T) &= g_0(T_{\text{ref}}/T)^n + g'_0(T_{\text{ref}}/T)^{n'}, \\ \delta_0(T) &= d_0(T_{\text{ref}}/T)^m + d'_0(T_{\text{ref}}/T)^{m'}, \\ \gamma_2(T) &= g_2(T_{\text{ref}}/T)^j + g'_2(T_{\text{ref}}/T)^{j'}, \\ \delta_2(T) &= d_2(T_{\text{ref}}/T)^k + d'_2(T_{\text{ref}}/T)^{k'}, \\ \tilde{\nu}_{\text{opt}}^r(T) &= r(T_{\text{ref}}/T)^p + r'(T_{\text{ref}}/T)^{p'}, \\ \tilde{\nu}_{\text{opt}}^i(T) &= i(T_{\text{ref}}/T)^q + i'(T_{\text{ref}}/T)^{q'}, \end{aligned} \quad (7)$$

where $T_{\text{ref}} = 296$ K. The full parametrization of the collisional line-shape effects requires 24 coefficients per single line, i.e., four coefficients per each of the six line-shape parameters, see Eqs. (7). It should be noted that Eqs. (7) represent the most general case of the DPL representation adopted in HITRAN [30]. For many molecular systems, not all the collisional effects are important at the considered accuracy level and, for a given experimental temperature range, a simple single-power law suffices. In such cases, one of the two approaches will be adopted in HITRAN. Either a single-power law and a smaller number of line-shape parameters will be stored (e.g., γ_0 and δ_0 for the simple Voigt profile or γ_0 , δ_0 , γ_2 and δ_2 for the quadratic speed-dependent Voigt profile) or the full DPL parametrization will be adopted but some of the 24 coefficients will be set to zero.

In this article, we show that our approach based on *ab initio* calculations allows us to fully benefit from the DPL parametrization given by Eqs. (7). We generated a comprehensive dataset of the beyond-Voigt line-shape parameters for a system for which all the six line-shape parameters are necessary to represent the shapes of molecular lines (i.e., He-perturbed H_2) and we use the DPL parametrization to represent these parameters in a wide temperature range, see Sec. III C for details.

The HITRAN DPL parametrization, see Eq. (7) and Ref. [30], does not use the exact form of the Hartmann-Tran profile (HT profile) [56] but its modified version, the qSDHC profile. The main difference between these profiles is that for the description of the velocity-changing collisions the HT profile uses the frequency of the velocity-changing collisions, $\tilde{\nu}_{\text{vc}}$, and the correlation parameter, η (first introduced by Rautian and Sobelmann [2]), while the qSDHC profile uses an explicit

parametrization with the real, $\tilde{\nu}_{\text{opt}}^r$, and imaginary, $\tilde{\nu}_{\text{opt}}^i$, parts of the complex Dicke parameter. The major advantage of the parametrization used in this work [30] is that it avoids singularities in temperature dependences of the complex Dicke parameter that may appear when the HT parametrization is used [30]. Another advantage of the qSDHC profile is that it does not require to introduce unphysical speed dependence of the complex Dicke parameter, in contrast to the original formulation of the HT profile. For details refer to the Appendices A and B in Ref. [30]; see also Ref. [57].

Hartmann proposed a different approach to populating spectroscopic databases with line-shape parameters based on *ab initio* calculations [58] (see also Sec. 2 in Ref. [30]). In his approach, the *ab initio* line-shape parameters are used with one of the sophisticated line-shape models to generate reference shapes in a wide range of pressures, and then the reference spectra are fitted with some simpler phenomenological model. In his scheme the fitted line-shape parameters lose their physical meaning but, in principle, the shapes of molecular lines should better agree with experiment. Similar tests were done before, for instance see Ref. [59] (in that work, due to a lack of *ab initio* parameters, a sophisticated line-shape model was used with parameters determined experimentally). Recently, this approach was tested for the requantized Classical Molecular Dynamics Simulations corrected with the use of experimental spectra [60]. However, in the case of the He-perturbed H_2 lines considered here, the difference between the qSDHC profile and the more sophisticated ones are much smaller than the difference with experimental data. Hence that approach [58] would not improve the accuracy of the dataset reported here.

III. ILLUSTRATION OF THE METHODOLOGY FOR THE CASE OF 2-0 Q(1) AND 3-0 S(1) LINES

In this section, we use an example of two rovibrational lines in He-perturbed H_2 to illustrate the methodology described in Sec. II and shown in Fig. 1. We consider the 2-0 Q(1) and 3-0 S(1) quadrupole lines that were recently accurately measured with the cavity enhanced techniques [31]; in this article we refer to them as reference lines. These measurements were used for accurate validation of the *ab initio* collisional line-shape calculations [31] and more recently these spectra were used for validation of improved quantum-scattering calculations that include centrifugal distortion [61].

A. *Ab initio* quantum scattering calculations

The H_2 -He PES is three-dimensional, i.e., it depends on the distance between the center of mass of the hydrogen molecule and the helium atom, R , the distance between the two hydrogen atoms, r , and the angle between the intra- and intermolecular axes, θ . The quantum-

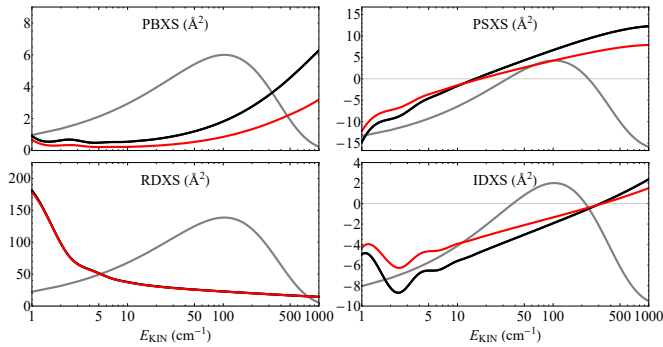


FIG. 2. Examples of the generalized spectroscopic cross sections for the case of 2-0 Q(1) and 3-0 S(1) lines in helium-perturbed H_2 , see the red and black lines, respectively. The four panels show the pressure broadening (PBXS), pressure shift (PSXS), and real (RDXS) and imaginary (IDXS) parts of the complex Dicke cross-sections as a function of collision energy. The gray line is the Maxwell-Boltzmann distribution at 296 K in arbitrary units.

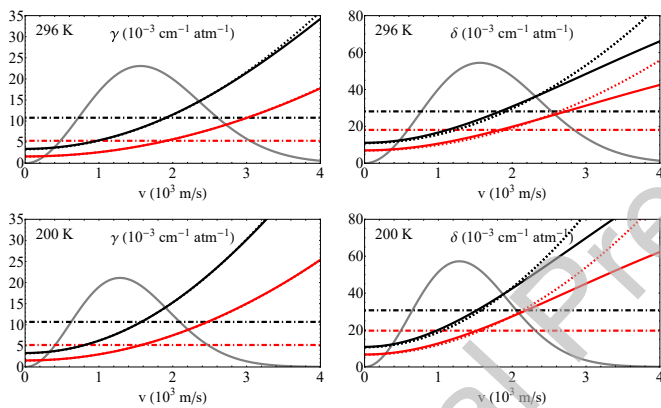


FIG. 3. Examples of the speed dependences of the broadening, γ , and shift, δ , parameters. The red and black lines correspond to the 2-0 Q(1) and 3-0 S(1) lines in helium-perturbed H_2 , respectively. The solid lines show the full *ab initio* results and the dotted lines show the quadratic approximations. The dash-dotted lines show the corresponding speed-averaged values. The calculations were done for $T = 296$ K (upper panels) and 200 K (lower panels); the corresponding Maxwell-Boltzmann distributions (in arbitrary units) are plotted as a gray lines.

scattering calculations [15, 26] that we used to generate the line-shape parameter dataset are based on the recent state-of-the-art PES that is an extension of the PES published by Bakr, Smith and Patkowski [14] (this PES will be referred to as BSP). The BSP PES was calculated using the coupled-cluster method with single, double and perturbative triple (CCSD(T)) excitations, taking into account also the contributions from the higher coupled-cluster excitations. It was determined for ten intramolecular separations, between 1.1 and 1.75 a_0 , which was shown to be insufficient for the detailed studies of processes involving the vibrationally excited H_2 molecule

(see Sec. 2 of Ref. [46] and Appendix C of [15] for details). This issue was addressed in the second version of this PES, BSP2, which extended the range of *ab initio* data points to $r \in [0.65, 3.75] a_0$. The final version of this PES, BSP3 [15], which was used in this work, has improved asymptotic behavior of the H_2 -He interaction energy at large R . The quantum scattering calculations based on the BSP3 PES were recently tested on highly accurate cavity-enhanced measurements of the shapes of He-perturbed H_2 2-0 Q(1) and 3-0 S(1) lines [31] resulting in unprecedented agreement between experimental and theoretical collision-induced line shapes. Furthermore, the BSP3 PES was employed in the studies of purely rotational lines of He-perturbed isotopologues of molecular hydrogen: D_2 [47, 62] and HD [63, 64].

For the purpose of dynamical calculations [15, 26], the three-dimensional H_2 -He PES is projected over Legendre polynomials, P_ξ [15, 26, 46]:

$$V(R, r, \theta) = \sum_{\xi} v_{\xi}(R, r) P_{\xi}(\cos \theta). \quad (8)$$

In the case of homonuclear molecules like H_2 , the ξ index takes only even values. Due to the small overall anisotropy of the H_2 -He PES, only the first four ξ values are retained throughout the calculations. The $v_{\xi}(R, r)$ terms are averaged over rovibrational wavefunctions of the unperturbed molecule, $\chi_{v,J}(r)$, leading to the radial coupling terms, $A_{\xi,v,J,v',J'}(R)$, which enter the close-coupled equations. At room temperature the vibrational coupling ($v \neq v'$) can be neglected [15, 26]. The influence of the centrifugal distortion (the J dependence of the radial coupling terms) was usually neglected in the scattering calculations for the rovibrational transitions [15, 26], as it was suggested that this effect might be masked due to the large contribution from the vibrational dephasing [46]. However, it was shown recently [61, 64] that if one aims for sub-percent accuracy of the line-shape parameters, the centrifugal distortion of the potential energy surface must be taken into account. Therefore, the J -dependence of the radial coupling terms $A_{\xi,v,J,v',J'}(R)$ was included in the following analysis.

The scattering calculations were performed using the recently developed BIGOS code [65] for a wide range of relative kinetic energies. The BIGOS code solves the coupled equations in the body-fixed frame of reference using the renormalized Numerov's algorithm [66]. Calculations were carried out for intermolecular distances ranging from 1 to 200 a_0 and three asymptotically closed levels were kept in the basis set. Figure 2 presents an example of the generalized spectroscopic cross sections for the 2-0 Q(1) and 3-0 S(1) lines.

B. Speed dependence of the broadening and shift, and the quadratic approximation

The calculations of the γ_0 , δ_0 , $\tilde{\nu}_{\text{opt}}^r$ and $\tilde{\nu}_{\text{opt}}^i$ parameters are straightforward and require only performing the

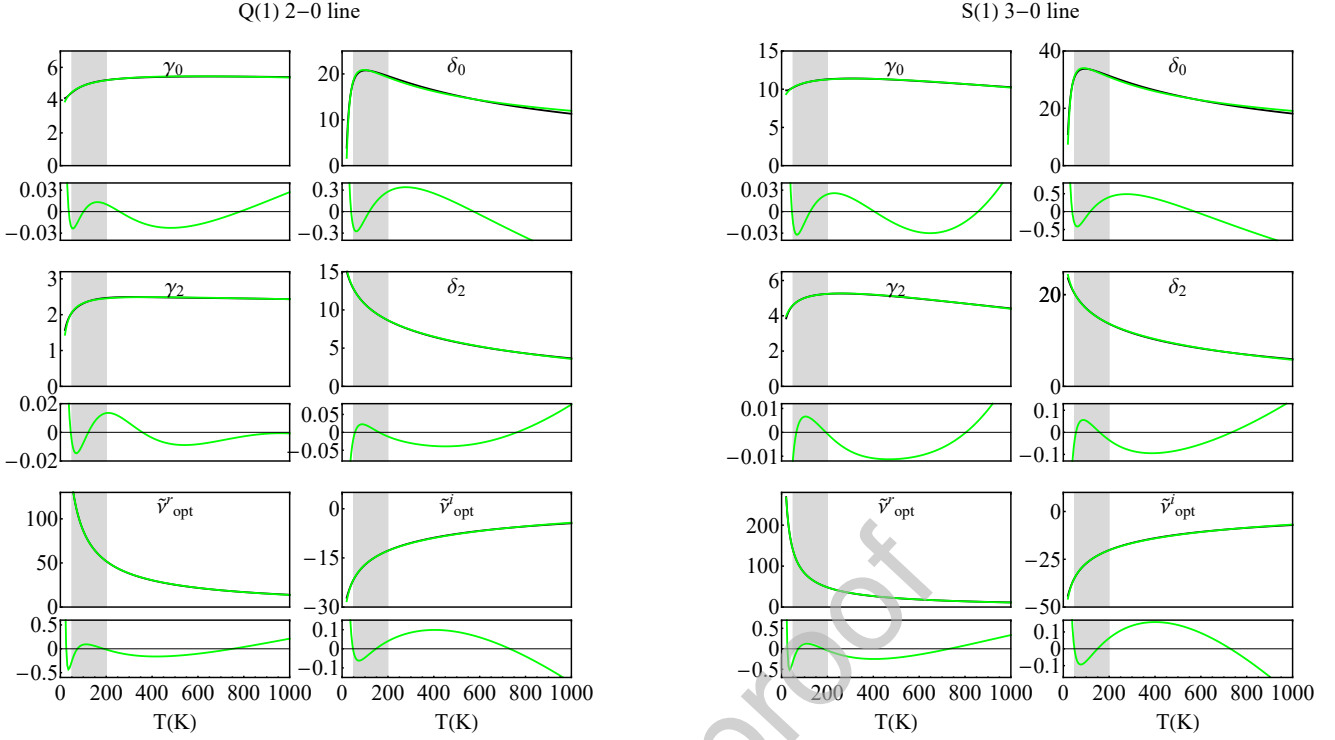


FIG. 4. Examples of the temperature dependences of the six collisional line-shape parameters, γ_0 , δ_0 , γ_2 , δ_2 , \tilde{v}_{opt}^r and \tilde{v}_{opt}^i , for the cases of the Q(1) 2-0 and S(1) 3-0 lines in H_2 perturbed by He. The black and green lines are the *ab initio* results and DPL approximations, respectively. The small panels show the residuals from the DPL fits. The vertical axes for all the panels (including residuals) are in $10^{-3}\text{cm}^{-1}\text{atm}^{-1}$. The gray shadows indicate the temperature range prioritized in the DPL fits; this temperature range is relevant for the atmospheres of giant planets.

averaging (with proper weights) of the generalized spectroscopic cross sections over the Maxwell distribution of the relative kinetic energy of a collision, see Eqs. (2) and (4). Calculations of the speed-dependence parameters, γ_2 and δ_2 , are, in principle, more complex and require a few additional steps. First, the *ab initio* speed-dependent broadening and shift are calculated from Eq. (1); Fig. 3 shows the result for the case of the 2-0 Q(1) and 3-0 S(1) lines. The full speed dependences are approximated with a quadratic function, see Eq. (3). The choice of how the γ_2 and δ_2 parameters are determined is not unique [67, 68]. In our methodology we demand that the slopes of the *ab initio* and quadratic speed dependences are equal at the most probable speed, see Eq. (5). This approach is very efficient from a computational perspective. The derivative from Eq. (5) can be done analytically before the integration in Eq. (1) and, hence, the γ_2 and δ_2 parameters can be evaluated directly by averaging the σ_0^q

cross section with proper weights

$$\gamma_2 + i\delta_2 = \frac{1}{2\pi c} \frac{1}{k_B T} \frac{\bar{v}_p}{\sqrt{\pi}} e^{-y^2} \times \int_0^\infty \left(2x \cosh(2xy) - \left(\frac{1}{y} + 2y \right) \sinh(2xy) \right) \times x^2 e^{-x^2} \sigma_0^q(x\bar{v}_p) dx, \quad (9)$$

where $x = v_r/\bar{v}_p$ and $y = v_m/\bar{v}_p$, with v_r , v_m and \bar{v}_p being the relative absorber to perturber speed, most probable absorber speed and most probable perturber speed, respectively. Note that $y = \sqrt{\alpha}$, where α is the perturber-to-absorber mass ratio. The quadratic approximations for the 2-0 Q(1) and 3-0 S(1) transitions are shown in Fig. 3 as dotted lines. The results from Fig. 3 were calculated for $T = 296$ K. The accuracy of the quadratic approximation depends on the choice of transition and line-shape parameter. In the cases considered in Fig. 3, the approximation works better for the γ parameter.

C. Temperature dependences of the line-shape parameters

The values of the six collisional line-shape parameters, γ_0 , δ_0 , γ_2 , δ_2 , $\tilde{\nu}_{\text{opt}}^r$ and $\tilde{\nu}_{\text{opt}}^i$, were calculated in the temperature range from 20 to 1000 K using Eqs. (4), (9) and (2). The examples of these results, for the case of our reference lines, are shown in Fig. 4. To represent these temperature dependences in the HITRAN database, we use the recently recommended DPL approximation [30] for all the six line-shape parameters, see Eqs. (7). The DPL fits were done for the 20 – 1000 K temperature range enforcing ten times larger fitting weights for the prioritized temperature range from 50 to 200 K (see the gray shadows in Fig. 4), which is relevant for the atmospheres of giant planets. The examples of the DPL fits are shown in Fig. 4 as green lines. The DPL approximation performs best when the temperature dependence is monotonic; when an extremum is clearly seen then the accuracy is worse, see the δ_0 panels in Fig. 4. The amplitude of the residuals for most of the cases is smaller than 1%; their exact values are taken into account in the estimations of the line-shape parameter uncertainties reported in our dataset, see the supplementary materials [34].

D. Examples of a complete dataset record

In Table I, we show examples of complete records from our line-shape parameter dataset for the cases of the two reference lines. All the coefficients are defined by Eqs. (7), following the original formulation from Ref. [30]. A set of 24 coefficients per a single molecular transition is required for a full DPL description of the six line-shape parameters. The values of the coefficients gathered in Table I are directly taken from the fits shown in Fig. 4. Note that at $T = T_{\text{ref}}$, Eqs. (7) simplify and a given line-shape parameter is simply a sum of the corresponding Coefficient 1 and Coefficient 2; for instance $\gamma_0(T_{\text{ref}}) = g_0 + g'_0$.

E. Experimental validation

In this section, we show experimental validation of our line-shape parameter dataset for the cases of the two reference lines. We use the experimental data reported in Ref. [31]. The 2-0 Q(1) line was measured in the Grenoble laboratory at nine pressures from 0.39 to 1.05 atm and at a temperature of 294.2 K. The 3-0 S(1) line was measured in the Hefei laboratory at four pressures from 0.36 to 1.35 atm and at temperature of 296.6 K. The experimental spectra are shown as black dots in Fig. 5. Both experiments are based on high-finesse cavity ring-down spectrometers; the experimental details are given in Ref. [31].

It was demonstrated in Ref. [31] that the synthetic profiles based on the fully *ab initio* calculations agree ex-

ceptionally well with the experimental profiles without fitting any of the line-shape parameters. The relative root mean square error (rRMSE) averaged over the pressures calculated within \pm FWHM around the line center was 0.33% and 0.99% for the 2-0 Q(1) and 3-0 S(1) lines, respectively [31]. Recently, the agreement with these experimental profiles was confirmed with an improved theoretical approach that includes the centrifugal distortion in the quantum-scattering calculation; rRMSE was 0.38% and 0.86% for the 2-0 Q(1) and 3-0 S(1) lines, respectively [61]. In this section, we show that we can reach an almost equally good agreement if we replace the full *ab initio* model with the approximate approach presented in this article, consistent with the HITRAN-format DPL parametrization [30]. The approximation is twofold. First, the full line-shape model [31, 53, 69] is replaced with a quadratic speed-dependent hard-collision (qSDHC) model. Second, the full *ab initio* temperature dependences are approximated with DPL. The comparison is shown in Fig. 5. The average rRMSE is 0.46% and 0.93% for the 2-0 Q(1) and 3-0 S(1) lines, respectively. It should be emphasized that none of the line-shapes were fitted in this comparison (all of them were taken from our dataset). For this comparison, we only fitted the line area, baseline, background slope and line center (all the pressures were fitted simultaneously and the fitted line center was constrained to be the same for all the pressures). The profiles from Fig. 5 were calculated using the β correction [25, 55] to the qSDHC profile, see Sec. II for details. Without the β correction, the average rRMSE considerably deteriorates and equals 1.43% and 1.08% for the 2-0 Q(1) and 3-0 S(1) lines, respectively.

IV. COMPREHENSIVE DATASET OF BEYOND VOIGT LINE-SHAPE PARAMETERS FOR THE HELIUM-PERTURBED H₂ LINES

In this section, we discuss the main result of the present paper, i.e., the complete dataset of the beyond-Voigt line-shape parameters for the He-perturbed H₂ rovibrational lines. We provide a full set of the line-shape parameters for all the 3480 H₂ rovibrational electric quadrupole lines present in the HITRAN database [24]. For our basic set of 321 lines (that contains the strongest lines) we directly perform *ab initio* calculations of the generalized spectroscopic cross sections, see Sec. III A. For all the other lines (higher overtones, high-J lines and high- ν' hot bands) we extrapolate the *ab initio* data. The majority of the extrapolated data concerns the hot bands. In this work, we extended the *ab initio* calculations from Refs. [15, 26] by taking into account the centrifugal distortion for all the bands and by including the hot bands. We also performed *ab initio* calculations for several dozen other lines with high ν or J numbers, which we use to adjust and validate our extrapolation scheme.

We use our *ab initio* generalized spectroscopic cross sections to calculate the line-shape parameters and their

TABLE I. Examples of the complete records from our DPL line-shape parameter dataset for the cases of the Q(1) 2-0 and S(1) 3-0 lines in H₂ perturbed by He. Coefficients 1 and 2 are in cm⁻¹atm⁻¹. Exponents 1 and 2 are dimensionless. All the DPL coefficients are defined by Eqs. (7), following the original formulation from Ref. [30].

Q(1) 2-0 line				
	Coefficient 1	Coefficient 2	Exponent 1	Exponent 2
$\gamma_0(T)$	$g_0 = 0.29611$	$g'_0 = -0.29076$	$n = -0.30724$	$n' = -0.31188$
$\delta_0(T)$	$d_0 = 1.29146$	$d'_0 = -1.27385$	$m = 0.617$	$m' = 0.622$
$\gamma_2(T)$	$g_2 = 0.114102$	$g'_2 = -0.111618$	$j = 0.2396$	$j' = 0.2453$
$\delta_2(T)$	$d_2 = 0.091305$	$d'_2 = -0.083861$	$k = -0.0013$	$k' = -0.0383$
$\tilde{\nu}_{opt}^r(T)$	$r = 0.04277$	$r' = -0.00417$	$p = 0.6856$	$p' = -0.1236$
$\tilde{\nu}_{opt}^i(T)$	$i = -0.27435$	$i' = 0.26376$	$q = 0.07106$	$q' = 0.05273$

S(1) 3-0 line				
	Coefficient 1	Coefficient 2	Exponent 1	Exponent 2
$\gamma_0(T)$	$g_0 = 0.012847$	$g'_0 = -0.001465$	$n = -0.11276$	$n' = -0.92775$
$\delta_0(T)$	$d_0 = 1.87405$	$d'_0 = -1.84585$	$m = 0.61066$	$m' = 0.61600$
$\gamma_2(T)$	$g_2 = 0.0493132$	$g'_2 = -0.0440504$	$j = -0.34485$	$j' = -0.38797$
$\delta_2(T)$	$d_2 = 1.5985$	$d'_2 = -1.5867$	$k = -0.01288$	$k' = -0.01602$
$\tilde{\nu}_{opt}^r(T)$	$r = 0.05173$	$r' = -0.01689$	$p = 0.6530$	$p' = 0.2554$
$\tilde{\nu}_{opt}^i(T)$	$i = -0.4136$	$i' = 0.39691$	$q = 0.08613$	$q' = 0.06746$

temperature dependences within the HITRAN DPL parametrization [30]. Our *ab initio* calculations of the cross sections were performed for:

- 105 lines from the Q-branches (J'' ranging from 1 to 7; Q(0) is forbidden) from the $\nu' - \nu''$ bands, with $\nu'' = 0, \dots, 4$ and $\Delta\nu = \nu' - \nu'' = 1, \dots, 5$,
- 126 lines from the S-branches (J'' ranging from 0 to 5) from the $\nu' - \nu''$ bands, with $\nu'' = 0, \dots, 5$ and $\Delta\nu = \nu' - \nu'' = 0, \dots, 5$,
- 90 lines from the O-branches (J'' ranging from 2 to 7) from the $\nu' - \nu''$ bands, with $\nu'' = 0, \dots, 4$ and $\Delta\nu = \nu' - \nu'' = 1, \dots, 5$.

For each of these 321 lines, we employ the methodology introduced in Sec. II to populate a complete dataset record defined by Eqs. (7) and illustrated in Table I.

In Figure 6, we show an example of the vibrational, ν' , and rotational, J'' , quantum number dependences of the line-shape parameters generated from our dataset at 150 K and 296 K (the plots do not show the raw *ab*

initio data, but the line-shape parameters already reconstructed from our HITRAN-format DPL dataset). We observe a strong dependence of all the six line-shape parameters on the vibrational number ν' , and much weaker dependence on the rotational number J'' , which is consistent with the phenomenological dataset for self-perturbed H₂ [25]. In Figure 7, we show the results for different hot bands; the colors indicate the change of the vibrational quantum number $\Delta\nu = \nu' - \nu''$. In contrast to the simplest assumption that for a fixed $\Delta\nu$ the line-shape parameters should hardly depend on ν'' (this was assumed, for instance, in the phenomenological database for the self-perturbed H₂ [25]), we observe a strong dependence on ν'' , especially for small $\Delta\nu$ for the γ_0 parameter.

The rovibrational lines in H₂ are exceptionally weak; the strongest line at $T = T_{\text{ref}} = 296$ K is the 1-0 S(1) line with a line intensity of 3.2×10^{-26} cm/molecule. The intensity quickly decreases with J'' and ν' . For instance, the intensity of the 1-0 S(5) line is as small as 2.2×10^{-29} cm/molecule, and the intensity of the 5-0 S(1) line is 0.95×10^{-29} cm/molecule. At lower temperatures

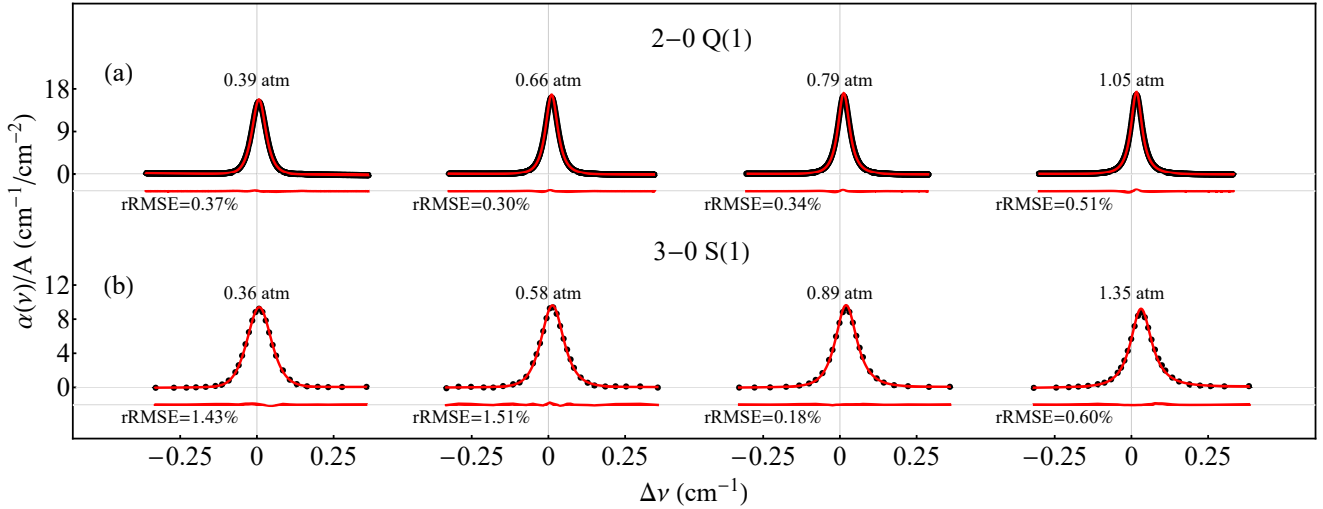


FIG. 5. Comparison of the synthetic spectra of the He-perturbed H_2 lines generated from our DPL HITRAN-format line-shape dataset (red lines) with experimental spectra (black points) collected with cavity ring-down spectrometers. Temperatures for the experimental and synthetic spectra are 294.2 K and 296.6 K for the 2-0 Q(1) and 3-0 S(1) lines, respectively. The red lines below the profiles show the differences between the experimental and synthetic spectra; rRMSE is the corresponding relative root mean square error calculated within $\pm\text{FWHM}$ around line center (relative means that RMSE is divided by the absorption coefficient at the line peak).

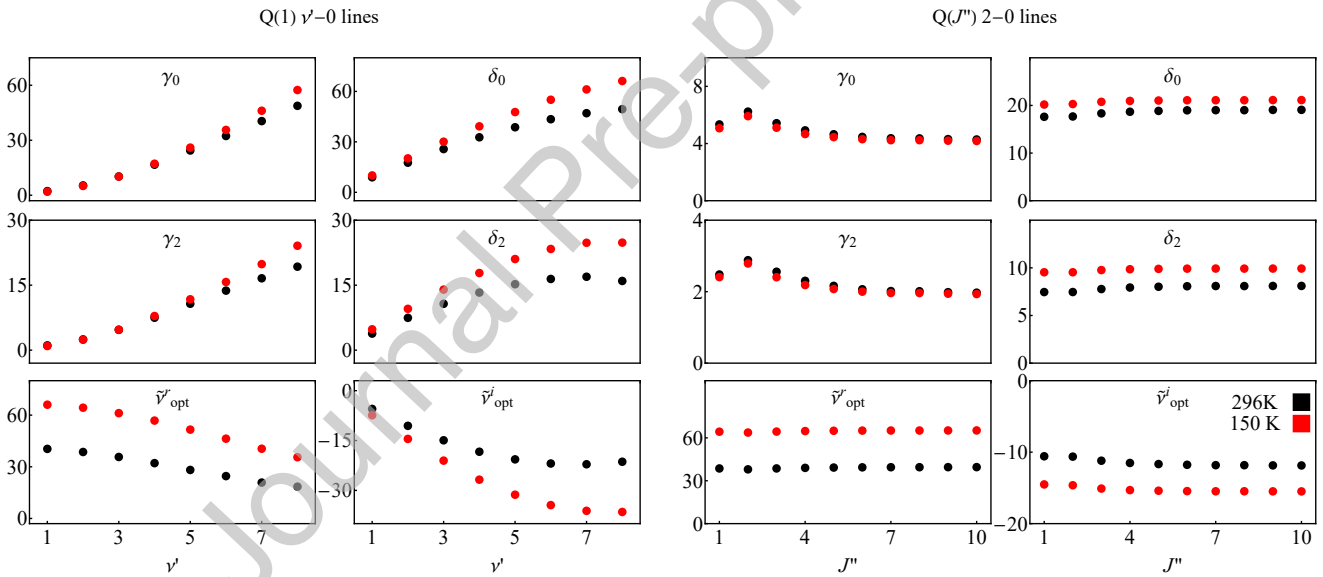


FIG. 6. An excerpt from our dataset illustrating the structure of the dataset and the examples of the vibrational and rotational dependences of all six line-shape parameters. The line-shape parameters are determined for the He-perturbed H_2 rovibrational lines at $T = 150$ and 296 K; refer to red and black colors, respectively. All the parameters are expressed in units of $10^{-3} \text{ cm}^{-1} \text{ atm}^{-1}$. The values of the line-shape parameters shown in this plot are not directly taken from *ab initio* calculations, but reconstructed from the DPL relations, Eqs. (7), based on the coefficients from our dataset [34].

that are relevant for giant planet atmospheres, the line intensity decreases with J'' and ν' even faster. For this reason, we limit our full line-shape calculations based on the *ab initio* generalized spectroscopic cross sections to $J'' < 8$ and $\nu' < 6$. For the completeness of the dataset, we extrapolate our calculations for higher J'' and ν' lines that are present in HITRAN (in fact, in this procedure

we combine extrapolation and interpolation). The extrapolation scheme is as follows. For every branch (O, Q and S), we calculated the values of the line-shape parameters for one high- ν' line per cold/hot band, i.e., we performed additional *ab initio* calculations for the following lines: Q(1) 9- x , S(1) 9- x , O(3) 9- x , with $x = 0, \dots, 5$. We assumed in our extrapolation that the proportions

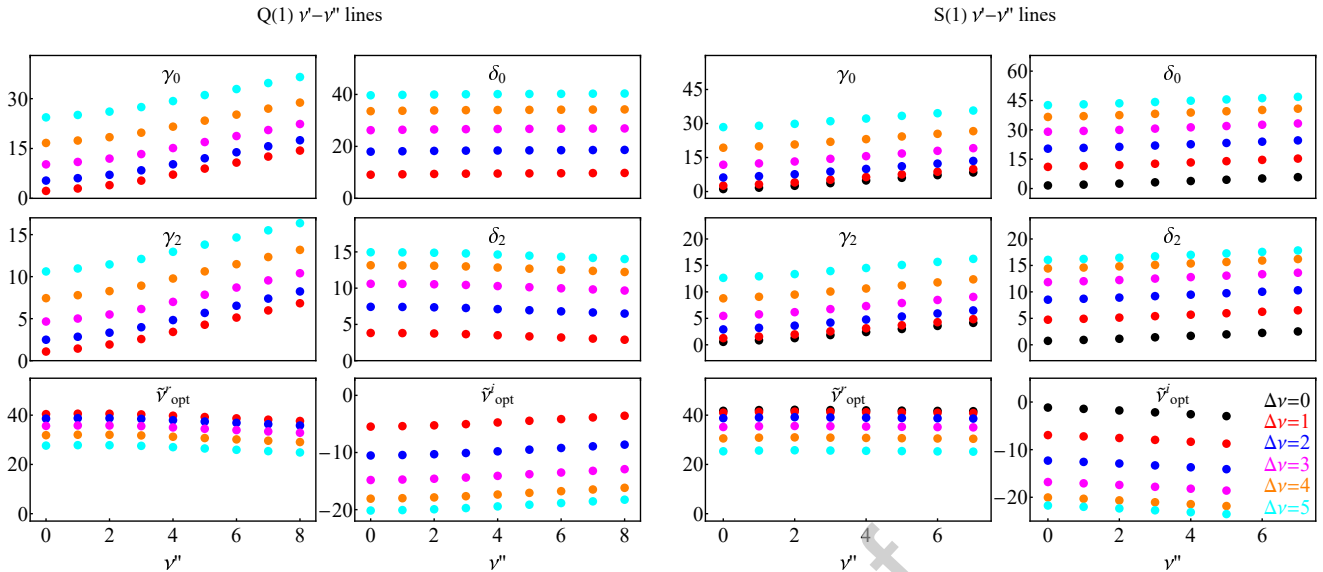


FIG. 7. An excerpt from our dataset illustrating the values of the beyond-Voigt line-shape parameters for different hot bands. The left and right sides of the figure show the results for the Q(1) and S(1) lines, respectively. All the parameters are expressed in units of $10^{-3} \text{ cm}^{-1} \text{ atm}^{-1}$. The values of the line-shape parameters shown in this plot are not directly taken from *ab initio* calculations, but reconstructed from the DPL relations, Eqs. (7), based on the coefficients from our dataset [34]. The data for $\nu' = \nu'' + \Delta\nu \geq 6$ come from extrapolation.

of the values of the line-shape parameters between the 9-0 and 5-0 bands for other J'' are the same as for the three cases mentioned above (i.e., the same within each branch). In the next step, we interpolated the line-shape parameters for the bands between 5-0 and 9-0 using a quadratic function fitted (separately for every J'') to 4-0, 5-0 and 9-0 data. The same approach was applied to extrapolate the data for hot bands. To populate the dataset for higher J'' , we performed fully *ab initio* calculations for the six high- J'' transitions belonging to the 2-0 band: O(10), O(13), Q(8), Q(11), S(8) and S(11) lines. We constrained the same proportions of the line-shape parameters between $J'' = 5, 8$ and 11 (10 and 13 for O branches) for other bands, and we interpolated the values of the line-shape parameters between $J'' = 5$ and 11 (13 for the O bands) with a quadratic function. For $J'' > 11$ ($J'' > 13$ for the O bands) we used linear extrapolation based on the last two J'' . This approach (based on the data for the 2-0 band) was used to extrapolate the data for higher J'' for all cold and hot bands. The scheme of data interpolation and extrapolation described above was implemented directly to the raw *ab initio* data before fitting the DPL temperature dependences. The reason for this is that the four DPL coefficients are strongly correlated with each other, and even for neighboring J'' and ν' quantum numbers their fitted values can be very different despite similar temperature dependences.

Due to a strong numerical correlation between the DPL coefficients, the uncertainties of the DPL coefficients do not suffice and a full covariance matrix would be needed. For this reason, we do not report an individual uncertainty for every DPL coefficient, but a single uncertainty

for the entire DPL function for a given line-shape parameter. The uncertainty consists of two contributions, the first one comes from the DPL approximation, and the second one from *ab initio* calculations. We calculate the DPL contribution as a standard deviation of the difference between the full *ab initio* values of the line-shape parameter and their DPL approximation calculated in the range from 50 to 200 K, see the small panels in Fig. 4. We estimate the uncertainty of our *ab initio* calculations at 1%.

The complete dataset of the line-shape parameters within the DPL representation [30] for the He-perturbed H_2 lines is given in the supplementary materials [34]; the definition of the reported coefficients is given by Eqs. (7). The lines are ordered with increasing transition energy. The above described format of the uncertainties reported in this work does not fit the standard HITRAN uncertainty codes. For this reason, the error codes in HITRAN will be set to *unreported* (code = 0). Nevertheless, all the uncertainties are reported in the supplementary materials [34] in the columns labelled *DPL-err*. In the supplementary materials [34], we also provide the source *ab initio* data that were used to generate the DPL dataset, i.e., the generalized spectroscopic cross sections and line-shape parameters as a function of temperature.

V. CONCLUSION

We demonstrated a methodology for populating line-by-line spectroscopic databases with beyond-Voigt line-shape parameters that is based on *ab initio* quantum

scattering calculations. We provided a comprehensive dataset for the benchmark system of He-perturbed H_2 (we cover all the rovibrational bands that are present in HITRAN). We extended the previous quantum-scattering calculations by taking into account the centrifugal distortion for all the bands and by including the hot bands. The results were projected on a simple structure of the quadratic speed-dependent hard-collision profile. For each line and each line-shape parameter, we provided a full temperature dependence within the double-power-law (DPL) representation. The temperature dependences cover the range from 20 to 1000 K, which also includes the low temperatures relevant for the studies of the atmospheres of giant planets. We demonstrated that the synthetic spectra generated from our dataset agree with highly accurate experimental spectra collected with cavity ring-down spectrometers at a subpercent accuracy level. The methodology can be applied to many other molecular species important for atmospheric and planetary studies.

ACKNOWLEDGEMENTS

P.W. was supported by Polish National Science Centre Project No. 2019/35/B/ST2/01118. N.S. and H.J. were supported by Polish National Science Centre Project No. 2018/31/B/ST2/00720. M.S., M.G. and K.S. were supported by the A next-generation worldwide quantum sensor network with optical atomic clocks project carried out within the TEAM IV Programme of the Foundation for Polish Science cofinanced by the European Union under the European Regional Development Fund. S.K. and A.C. acknowledge funding support from the Agence Nationale de la Recherche (Equipex REFIMEVE+ANR-11-EQPX-0039). M.K. and D.L. were supported by Polish National Science Centre Project No. 2015/18/E/ST2/00585. K.P. was supported by U.S. National Science Foundation CAREER award CHE-1351978. The project was cofinanced by the Polish National Agency for Academic Exchange under the PHC Polonium program (dec. PPN/X/PS/318/2018). The research was part of the program of the National Laboratory FAMO in Toruń, Poland. The HITRAN database is supported by NASA AURA NNX17AI78G and NASA PDART NNX16AG51G grants.

-
- [1] R. Dicke, *Phys. Rev.* **89**, 472 (1953), URL <http://link.aps.org/doi/10.1103/PhysRev.89.472>.
- [2] S. G. Rautian and I. I. Sobelman, *Usp. Fiz. Nauk* **90**, 209 (1966) [*Sov. Phys. Usp.* **9**, 701 (1967)] ().
- [3] P. R. Berman, *J. Quant. Spectrosc. Radiat. Transfer* **12**, 1331 (1972), ISSN 0022-4073, URL <http://www.sciencedirect.com/science/article/pii/0022407372901896>.
- [4] S. Hess, *Physica* **61**, 80 (1972), ISSN 0031-8914, URL <http://www.sciencedirect.com/science/article/pii/0031891472900353>.
- [5] R. Blackmore, *J. Chem. Phys.* **87**, 791 (1987), URL <http://scitation.aip.org/content/aip/journal/jcp/87/2/10.1063/1.453286>.
- [6] R. Ciuryło, A. Bielski, J. R. Drummond, D. Lisak, A. D. May, A. S. Pine, D. A. Shapiro, J. Szudy, and R. S. Trawiński, *Spectral Line Shapes*, edited by C. A. Back (AIP, Melville, NY, 2002) p. 151 (2002).
- [7] A. D. May, W.-K. Liu, F. R. W. McCourt, R. Ciuryło, J. Sanchez-Fortn Stoker, D. Shapiro, and R. Wehr, *Can. J. Phys.* **91**, 879 (2013), URL <http://dx.doi.org/10.1139/cjp-2012-0345>.
- [8] J.-M. Hartmann, H. Tran, N. H. Ngo, X. Landshere, P. Chelin, Y. Lu, A.-W. Liu, S.-M. Hu, L. Gianfrani, G. Casa, et al., *Phys. Rev. A* **87**, 013403 (2013), URL <http://link.aps.org/doi/10.1103/PhysRevA.87.013403>.
- [9] M. D. De Vizia, A. Castrillo, E. Fasci, P. Amodio, L. Moretti, and L. Gianfrani, *Phys. Rev. A* **90**, 022503 (2014), URL <https://link.aps.org/doi/10.1103/PhysRevA.90.022503>.
- [10] V. M. Devi, D. C. Benner, M. A. H. Smith, A. W. Mantz, K. Sung, T. J. Crawford, and A. Predoi-Cross, *J. Quant. Spectrosc. Radiat. Transfer* **152**, 149 (2015), URL <https://doi.org/10.1016/j.jqsrt.2014.11.011>.
- [11] A. Campargue, E. V. Karlovets, and S. Kassi, *J. Quant. Spectrosc. Radiat. Transfer* **154**, 113 (2015), URL <https://doi.org/10.1016/j.jqsrt.2014.12.011>.
- [12] S. Wójtewicz, P. Masłowski, A. Cygan, P. Wcisło, M. Zaborowski, M. Piwiński, R. Ciuryło, and D. Lisak, *J. Quant. Spectrosc. Radiat. Transfer* **165**, 68 (2015), URL <https://doi.org/10.1016/j.jqsrt.2015.06.022>.
- [13] V. T. Sironneau and J. T. Hodges, *J. Quant. Spectrosc. Radiat. Transfer* **152**, 1 (2015), URL <https://doi.org/10.1016/j.jqsrt.2014.10.020>.
- [14] B. W. Bakr, D. G. A. Smith, and K. Patkowski, *J. Chem. Phys.* **139**, 144305 (2013), URL <https://doi.org/10.1063/1.4824299>.
- [15] F. Thibault, K. Patkowski, P. S. Żuchowski, H. Józwiak, R. Ciuryło, and P. Wcisło, *J. Quant. Spectrosc. Radiat. Transfer* **202**, 308 (2017), ISSN 0022-4073, URL <http://www.sciencedirect.com/science/article/pii/S0022407317305058>.
- [16] P. Wcisło and R. Ciuryło, *J. Quant. Spectrosc. Radiat. Transfer* **120**, 36 (2013), ISSN 0022-4073, URL <http://www.sciencedirect.com/science/article/pii/S0022407313000782>.
- [17] P. Wcisło, F. Thibault, H. Cybulski, and R. Ciuryło, *Phys. Rev. A* **91**, 052505 (2015), URL <http://link.aps.org/doi/10.1103/PhysRevA.91.052505>.
- [18] P. Wcisło, I. E. Gordon, C.-F. Cheng, S.-M. Hu, and R. Ciuryło, *Phys. Rev. A* **93**, 022501 (2016), URL <https://link.aps.org/doi/10.1103/PhysRevA.93.022501>.
- [19] C. E. Miller, L. R. Brown, R. A. Toth, D. C. Benner, and V. M. Devi, *C. R. Phys.* **6**, 876 (2005), ISSN 1631-0705, URL <http://www.sciencedirect.com/science/>

- article/pii/S1631070505001155.
- [20] H. Feuchtgruber, E. Lellouch, G. Orton, T. de Graauw, B. Vandenbussche, B. Swinyard, R. Moreno, C. Jarchow, F. Billebaud, T. Cavalié, et al., *A&A* **551**, A126 (2013), URL <https://doi.org/10.1051/0004-6361/201220857>.
- [21] E. Miller-Ricci, S. Seager, and D. Sasselov, *Astrophys. J.* **690**, 1056 (2008), URL <https://doi.org/10.1088/0004-637x/690/2/1056>.
- [22] J. J. Fortney, T. D. Robinson, S. Domagal-Goldman, A. D. D. Genio, I. E. Gordon, E. Gharib-Nezhad, N. Lewis, C. Sousa-Silva, V. Airapetian, B. Drouin, et al., arXiv:1905.07064 (2019), URL <https://arxiv.org/abs/1905.07064>.
- [23] C. Hill, I. E. Gordon, R. V. Kochanov, L. Barrett, J. S. Wilzewski, and L. S. Rothman, *J. Quant. Spectrosc. Radiat. Transfer* **177**, 4 (2016), URL <http://www.sciencedirect.com/science/article/pii/S0022407315302375>.
- [24] I. Gordon, L. Rothman, C. Hill, R. Kochanov, Y. Tan, P. Bernath, M. Birk, V. Boudon, A. Campargue, K. Chance, et al., *J. Quant. Spectrosc. Radiat. Transfer* **203**, 3 (2017), URL <http://www.sciencedirect.com/science/article/pii/S0022407317301073>.
- [25] P. Weislo, I. Gordon, H. Tran, Y. Tan, S.-M. Hu, A. Campargue, S. Kass, D. Romanini, C. Hill, R. Kochanov, et al., *J. Quant. Spectrosc. Radiat. Transfer* **177**, 75 (2016), URL <http://www.sciencedirect.com/science/article/pii/S0022407315302028>.
- [26] H. Jóźwiak, F. Thibault, N. Stolarczyk, and P. Weislo, *J. Quant. Spectrosc. Radiat. Transfer* **219**, 313 (2018), URL <http://www.sciencedirect.com/science/article/pii/S002240731830428X>.
- [27] A. S. Pine, *J. Quant. Spectrosc. Radiat. Transfer* **62**, 397 (1999), ISSN 0022-4073, URL <http://www.sciencedirect.com/science/article/pii/S0022407398001125>.
- [28] N. Ngo, D. Lisak, H. Tran, and J.-M. Hartmann, *J. Quant. Spectrosc. Radiat. Transfer* **129**, 89 (2013), ISSN 0022-4073, URL <http://www.sciencedirect.com/science/article/pii/S0022407313002422>.
- [29] J. Tennyson, P. F. Bernath, A. Campargue, A. G. Csaszr, L. Daumont, R. R. Gamache, J. T. Hodges, D. Lisak, O. V. Naumenko, L. S. Rothman, et al., *Pure Appl. Chem.* **86**, 1931 (2014), URL <http://dx.doi.org/10.1515/pac-2014-0208>.
- [30] N. Stolarczyk, F. Thibault, H. Cybulski, H. Jóźwiak, G. Kowzan, B. Vispoel, I. E. Gordon, L. S. Rothman, R. R. Gamache, and P. Weislo, *J. Quant. Spectrosc. Radiat. Transfer* **240**, 106676 (2020), URL <http://www.sciencedirect.com/science/article/pii/S0022407319304480>.
- [31] M. Słowiński, F. Thibault, Y. Tan, J. Wang, A.-W. Liu, S.-M. Hu, S. Kass, A. Campargue, M. Konefał, H. Jóźwiak, et al., *Phys. Rev. A* **101**, 052705 (2020).
- [32] R. Kochanov, I. Gordon, L. Rothman, P. Weislo, C. Hill, and J. Wilzewski, *J. Quant. Spectrosc. Radiat. Transfer* **177**, 15 (2016), URL <http://www.sciencedirect.com/science/article/pii/S0022407315302466>.
- [33] E. Lellouch, B. Bézard, T. Fouchet, H. Feuchtgruber, T. Encrenaz, and T. de Graauw, *A&A* **370**, 610 (2001), URL <https://doi.org/10.1051/0004-6361:20010259>.
- [34] P. Weislo, F. Thibault, N. Stolarczyk, H. Jóźwiak, M. Słowiński, M. Gancewski, K. Stankiewicz, and K. M., Supplementary material (2020).
- [35] D. Long, D. Havey, M. Okumura, C. Miller, and J. Hodges, *J. Quant. Spectrosc. Radiat. Transfer* **111**, 2021 (2010), URL <http://www.sciencedirect.com/science/article/pii/S0022407310001809>.
- [36] V. M. Devi, D. C. Benner, M. Smith, A. Mantz, K. Sung, L. Brown, and A. Predoi-Cross, *J. Quant. Spectrosc. Radiat. Transfer* **113**, 1013 (2012), URL <http://www.sciencedirect.com/science/article/pii/S0022407312000696>.
- [37] V. M. Devi, D. C. Benner, M. A. H. Smith, A. W. Mantz, K. Sung, and L. R. Brown, *J. Mol. Spectrosc.* **276-277**, 33 (2012), URL <http://www.sciencedirect.com/science/article/pii/S002285212000872>.
- [38] G. Li, I. E. Gordon, P. G. Hajigeorgiou, J. A. Coxon, and L. S. Rothman, *J. Quant. Spectrosc. Radiat. Transfer* **130**, 284 (2013), URL <http://www.sciencedirect.com/science/article/pii/S0022407313003026>.
- [39] J. Domysawska, S. Wjtewicz, P. Masowski, A. Cygan, K. Bielska, R. S. Trawiski, R. Ciuryo, and D. Lisak, *J. Quant. Spectrosc. Radiat. Transfer* **169**, 111 (2016), ISSN 0022-4073, URL <http://www.sciencedirect.com/science/article/pii/S0022407315300820>.
- [40] D. C. Benner, C. P. Rinsland, V. M. Devi, M. A. H. Smith, and D. Atkins, *J. Quant. Spectrosc. Radiat. Transfer* **53**, 705 (1995), ISSN 0022-4073, URL <http://www.sciencedirect.com/science/article/pii/002240739500015D>.
- [41] A. Pine and R. Ciurylo, *J. Mol. Spectrosc.* **203**, 180 (2001), ISSN 0022-2852, URL <http://www.sciencedirect.com/science/article/pii/S002285201983754>.
- [42] P. Amodio, L. Moretti, A. Castrillo, and L. Gianfrani, *J. Chem Phys* **140**, 044310 (2014), URL <https://doi.org/10.1063/1.4862482>.
- [43] A. Ben-Reuven, *Phys. Rev.* **141**, 34 (1966), URL <http://link.aps.org/doi/10.1103/PhysRev.141.34>.
- [44] A. Ben-Reuven, *Phys. Rev.* **145**, 7 (1966), URL <http://link.aps.org/doi/10.1103/PhysRev.145.7>.
- [45] R. Shafer and R. G. Gordon, *J. Chem. Phys.* **58**, 5422 (1973), URL <https://doi.org/10.1063/1.1679162>.
- [46] F. Thibault, P. Weislo, and R. Ciurylo, *Eur. Phys. J. D* **70**, 236 (2016), URL <http://dx.doi.org/10.1140/epjd/e2016-70114-9>.
- [47] R. Z. Martínez, D. Bermejo, F. Thibault, and P. Weislo, *J. Raman Spectrosc.* **49**, 1339 (2018), URL <https://onlinelibrary.wiley.com/doi/abs/10.1002/jrs.5391>.
- [48] L. Monchick and L. W. Hunter, *J. Chem. Phys.* **85**, 713 (1986), URL <http://dx.doi.org/10.1063/1.451277>.
- [49] J. Schaefer and L. Monchick, *J. Chem. Phys.* **87**, 171 (1987), URL <https://doi.org/10.1063/1.453612>.
- [50] G. C. Corey and F. R. McCourt, *J. Chem. Phys.* **81**, 2318 (1984), URL <https://doi.org/10.1063/1.447930>.
- [51] J. Ward, J. Cooper, and E. W. Smith, *J. Quant. Spectrosc. Radiat. Transfer* **14**, 555 (1974), ISSN 0022-4073, URL <http://www.sciencedirect.com/science/article/pii/0022407374900363>.
- [52] D. Lisak, J. T. Hodges, and R. Ciurylo, *Phys. Rev. A* **73**, 012507 (2006), URL <https://link.aps.org/doi/10.1103/PhysRevA.73.012507>.
- [53] P. Weislo, F. Thibault, M. Zaborowski, S. Wójtewicz, A. Cygan, G. Kowzan, P. Masłowski, J. Komasa, M. Puchalski, K. Pachucki, et al., *J. Quant. Spec-*

- tros. Radiat. Transfer **213**, 41 (2018), ISSN 0022-4073, URL <http://www.sciencedirect.com/science/article/pii/S0022407318301341>.
- [54] F. Rohart, G. Włodarczak, J.-M. Colmont, G. Cazoli, L. Dore, and C. Puzzarini, *J. Mol. Spectrosc.* **251**, 282 (2008), ISSN 0022-2852, URL <http://www.sciencedirect.com/science/article/pii/S002228520800115X>.
- [55] M. Konefał, M. Słowiński, M. Zaborowski, R. Ciuryło, D. Lisak, and P. Wcisło, *J. Quant. Spectrosc. Radiat. Transfer* **242**, 106784 (2020), URL <http://www.sciencedirect.com/science/article/pii/S0022407319305795>.
- [56] H. Tran, N. Ngo, and J.-M. Hartmann, *J. Quant. Spectrosc. Radiat. Transfe* **129**, 199 (2013), ISSN 0022-4073, URL <http://www.sciencedirect.com/science/article/pii/S0022407313002598>.
- [57] G. Kowzan, P. Wciso, M. Sowiski, P. Masowski, A. Viel, and F. Thibault, *J. Quant. Spectrosc. Radiat. Transfer* **243**, 106803 (2020), ISSN 0022-4073, URL <http://www.sciencedirect.com/science/article/pii/S0022407319307277>.
- [58] *Private communication with J.-M. Hartmann* (2018).
- [59] P. Wcisło, D. Lisak, R. Ciuryło, and A. S. Pine, *J Phys: Conf Series* **810**, 012061 (2017), URL <https://doi.org/10.1088%2F1742-6596%2F810%2F1%2F012061>.
- [60] N. Ngo and J.-M. Hartmann, *J. Quant. Spectrosc. Radiat. Transfer* **203**, 334 (2017), ISSN 0022-4073, HITRAN2016 Special Issue, URL <http://www.sciencedirect.com/science/article/pii/S002240731730016X>.
- [61] M. Słowiński and et al., in preparation ().
- [62] R. Z. Martnez, D. Bermejo, P. Wciso, and F. Thibault, *J. Raman Spectrosc.* **50**, 127 (2019).
- [63] F. Thibault, R. Z. Martnez, D. Bermejo, and P. Wciso, *Mol. Astrophys.* **19**, 100063 (2020), ISSN 2405-6758, URL <http://www.sciencedirect.com/science/article/pii/S2405675820300014>.
- [64] K. Stankiewicz, H. Józwiak, M. Gancewski, N. Stolarczyk, F. Thibault, and P. Wcisło, *J. Quant. Spectrosc. Radiat. Transfer* **254**, 107194 (2020).
- [65] H. Józwiak, M. Gancewski, K. Stankiewicz, and P. Wcisło, *BIGOS computer code, to be published* ().
- [66] B. R. Johnson, *J. Chem. Phys.* **69**, 4678 (1978).
- [67] F. Rohart, L. Nguyen, J. Buldyreva, J.-M. Colmont, and G. Włodarczak, *J. Mol. Spectrosc.* **246**, 213 (2007), ISSN 0022-2852, URL <http://www.sciencedirect.com/science/article/pii/S0022285207002482>.
- [68] D. Lisak, A. Cygan, P. Wciso, and R. Ciuryło, *J. Quant. Spectrosc. Radiat. Transfer* **151**, 43 (2015), ISSN 0022-4073, URL <http://www.sciencedirect.com/science/article/pii/S0022407314003604>.
- [69] R. Ciuryło, D. A. Shapiro, J. R. Drummond, and A. D. May, *Phys. Rev. A* **65**, 012502 (2002), URL <http://link.aps.org/doi/10.1103/PhysRevA.65.012502>.

DECLARATION OF INTERESTS

The authors declare that they have no known competing financial interests or personal relationships that could have appeared to influence the work reported in this paper.

AUTHOR CONTRIBUTION

Piotr Wciso: Conceptualization, Methodology, Validation, Writing - original draft, Writing - review & editing Franck Thibault: Conceptualization, Methodology, Software, Validation, Writing - original draft, Writing - review & editing Nikodem Stolarczyk: Investigation, Visualization, Methodology, Software, Validation, Data Curation, Writing - original draft, Writing - review & editing Hubert Jwiak: Investigation, Methodology, Software, Validation, Data Curation, Writing - original draft, Writing - review & editing Micha Sowiski: Investigation, Visualization, Methodology, Software, Validation, Data Curation, Writing - original draft, Writing - review & editing Maciej Gancewski: Investigation, Software, Validation, Data Curation, Writing - original draft, Writing - review & editing Kamil Stankiewicz: Investigation, Software, Validation, Data Curation, Writing - original draft, Writing - review & editing Magdalena Konefa: Validation Samir Kassi: Investigation Alain Campargue: Investigation Yan Tan: Investigation Jin Wang: Investigation Konrad Patkowski: Investigation, Software, Writing - review & editing Roman Ciuryło: Conceptualization, Methodology, Writing - review & editing Daniel Lisak: Conceptualization, Methodology, Writing - review & editing Roman Kochanov: Conceptualization, Methodology, Data Curation Laurence Rothman: Conceptualization, Methodology, Data Curation, Validation, Writing - review & editing Iouli Gordon: Conceptualization, Methodology, Data Curation, Validation, Writing - review & editing